Doublon bound states in the continuum through giant atoms

Walter Rieck, ¹ Anton Frisk Kockum, ^{1,*} and Guangze Chen^{1,†}

¹Department of Microtechnology and Nanoscience,

Chalmers University of Technology, 41296 Gothenburg, Sweden

(Dated: November 25, 2025)

Bound states in the continuum (BICs) are spatially localized modes embedded in the spectrum of extended states, typically stabilized by symmetry or interference. While extensively studied in single-particle and linear systems, the many-body regime of BICs remains largely unexplored. Here, we demonstrate that giant atoms, quantum emitters coupled nonlocally to structured waveguides, can host robust doublon BICs, i.e., two-photon bound states stabilized by destructive interference and interactions. We first analyze a driven two-photon emission process and show how doublon BICs arise and mediate decoherence-free interaction between distant atoms. We then demonstrate that these many-body BICs also emerge under natural, undriven dynamics via a virtual two-photon emission process in three-level giant atoms. Our results reveal an interference-based mechanism for stabilizing many-body localization in open quantum systems, with potential applications in quantum simulation, non-ergodic dynamics, and protected quantum information processing.

Introduction.—Bound states in the continuum (BICs) are spatially localized eigenstates that exist within the continuous spectrum of extended, radiative modes [1, 2]. They can arise through mechanisms such as symmetry protection [3], separability of variables [4], or destructive interference between leakage channels [5–7]. BICs have been extensively studied in photonic and acoustic systems [8–13], where their unique combination of spatial confinement and spectral embedding gives rise to exceptionally long lifetimes and sharp resonances. Crucially, their in-band nature enables efficient coupling to external radiation or nearby modes, while their bounded character ensures strong field localization. These properties make BICs ideal platforms for many applications, including nonlinear optical enhancement [14-19], coherent light generation [20–23], and ultrasensitive sensing [24–28].

Recently, there has been growing interest in extending the concept of BICs to the many-body regime, where they could offer new mechanisms for suppressing thermalization [29]. However, this regime remains largely unexplored. Existing studies typically rely on impurity-induced localization [29–31], which requires engineered on-site potentials and is therefore experimentally challenging, or on boundary effects [32], where the resulting BICs are tied to the system's boundary and offer limited flexibility for applications. This motivates the search for new platforms and mechanisms to realize many-body BICs in a more controllable manner.

Giant atoms (GAs)—quantum emitters coupled to a waveguide at multiple, spatially separated points, have emerged in the past decade as a versatile platform for exploring nonlocal and interference-driven light-matter interactions [33]. As shown both theoretically [34–57] and experimentally for several systems [58–71], the nonlocal coupling of GAs results in interference effects that alter spontaneous emission and give rise to phenomena beyond conventional quantum optics. A striking example is the emergence of decoherence-free interaction

(DFI) [36, 63], where multiple GAs interact coherently through a waveguide without radiative losses into the waveguide. Notably, the DFI can be understood as a manifestation of BICs [38, 48, 51, 72], where destructive interference between emission pathways cancels radiation into the waveguide, forming long-lived collective modes. This connection highlights the potential of GAs to realize interference-based many-body BICs. However, studies of BICs in giant-atom systems have so far been restricted to the single-excitation regime, leaving the many-body dynamics and localization mechanisms unexplored.

In this Letter, we propose a mechanism to realize many-body BICs through destructive interference in giant-atom systems, focusing on the emergence of doublon BICs—two-photon bound states that remain localized despite lying within the radiation continuum of a structured waveguide. We begin by analyzing a driven two-photon emission process for a single two-level GA. demonstrating how these states arise from the interplay between interactions and interference, which suppresses decay into the waveguide. We then show that doublon BICs can mediate DFI between two GAs, reinforcing their physical significance. Going beyond this illustrative setup, we demonstrate that doublon BICs and their associated DFI can also emerge under undriven dynamics with realistic coupling configurations for three-level GAs. We finally discuss how our proposal can be realized on several experimental platforms and its potential applications in generating and distributing many-body entangled states.

Model.—We consider a system of multiple GAs coupled to a structured waveguide; see Fig. 1(a). The total Hamiltonian for this system is

$$H = H_A + H_B + H_{\text{int}},\tag{1}$$

where H_A and H_B are the bare Hamiltonians for the atoms and the bath (waveguide), respectively, and H_{int} describes their interaction.

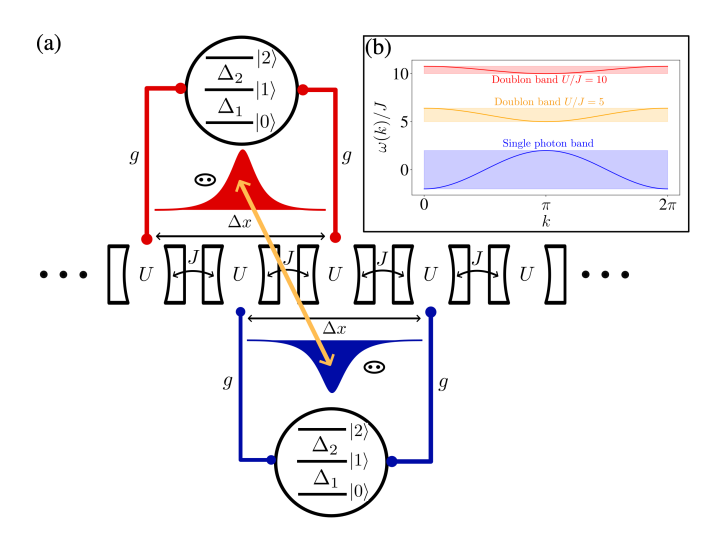


FIG. 1. Overview of the system. (a) Schematic of two three-level GAs coupled to a structured waveguide with nearest-neighbor hopping rate J and on-site two-photon interaction U. Each atom has level spacings detuned by $\Delta_{1,2}$ from the band center and is coupled to the waveguide at two points, spatially separated with distance $\Delta x = 2$, forming a braided configuration. The coupling strength at each connection point is g. For appropriate level spacings, doublon bound states in the continuum (BICs) emerge via interference between emission pathways. The overlap of these doublon BICs between the two atoms mediates a decoherence-free interaction (orange arrow). (b) Band structure of the nonlinear waveguide, for two different values of U.

The bath we consider is a one-dimensional array of N coupled cavities with nearest-neighbor hopping J and onsite Kerr nonlinearity U. Without loss of generality, we work in a frame rotating at ω_c , the center of the bath band. The bare bath Hamiltonian in this rotating frame is thus

$$H_B = \sum_{n=1}^{N} \frac{U}{2} a_n^{\dagger} a_n^{\dagger} a_n a_n - \sum_{n=1}^{N-1} J(a_n^{\dagger} a_{n+1} + \text{H.c.}), \quad (2)$$

where a_n (a_n^{\dagger}) is the photon annihilation (creation) operator for cavity n and H.c. denotes Hermitian conjugate.

The Kerr nonlinearity U supports the formation of doublons—two-photon bound states where the photons tend to stay near each other [30, 73–76]. A doublon with momentum k has the wavefunction [74, 75]

$$|\psi_D(k)\rangle = \frac{1}{\sqrt{2}} \sum_{m=1}^N \sum_{n=1}^N e^{ik\frac{(m+n)}{2}} e^{-\frac{|m-n|}{\varsigma(k)}} a_m^{\dagger} a_n^{\dagger} |\text{vac}\rangle \quad (3)$$

where $\varsigma(k)$ is the momentum-dependent localization length and $|\text{vac}\rangle$ is the vacuum state. These doublons can propagate through the waveguide and have the dispersion relation [74, 75]

$$\omega_D(k) = \operatorname{sign}(U)\sqrt{U^2 + 16J^2 \cos^2\left(\frac{k}{2}\right)}.$$
 (4)

Notably, when $U \geq 4J$, the doublon band becomes energetically separated from the continuum of two unbound photons; see Fig. 1(b). This separation allows us to isolate doublon-mediated dynamics by tuning the atomic level spacings to match the doublon dispersion.

Since our study involves multi-photon processes, we model each GA as a three-level system. For simplicity, we assume all atoms have an identical ladder-type level structure, with ω_1 (ω_2) the level spacing between the $|0\rangle$ ($|1\rangle$) and $|1\rangle$ ($|2\rangle$) levels of the atom. The bare Hamiltonian for N_a GAs is then, in the frame rotating at ω_c ,

$$H_A = \sum_{n=1}^{N_a} \left[(\Delta_2 + \Delta_1) \frac{\sigma_n^{(2),+} \sigma_n^{(2),-}}{2} + \Delta_1 \sigma_n^{(1),+} \sigma_n^{(1),-} \right],$$
(5)

where $\Delta_i = \omega_i - \omega_c$ and the ladder operators act as

$$\sigma_n^{(j),+}|j-1\rangle = \sqrt{j}|j\rangle, \quad \sigma_n^{(j),-}|j\rangle = \sqrt{j}|j-1\rangle.$$
 (6)

Direct two-photon emission.—The key ingredient of GAs is the multiple-point coupling: each GA n is coupled to the waveguide at p_n different cavities with strength g. To illustrate how this multi-point coupling can result in a doublon BIC, we first consider a direct two-photon emission process described by the interaction Hamiltonian

$$H_{\text{int}} = g \sum_{n=1}^{N_a} \sum_{j=1}^{p_n} \left[\sigma_n^{(1),+} a_{x_{nj}} a_{x_{nj}} + \text{H.c.} \right], \tag{7}$$

where x_{nj} is the jth coupling point of atom n. Although we here mostly use this type of nonlinear coupling for illustrative purposes, it can be engineered experimentally using external drives [77]. If the two-photon operator in Eq. (7) is replaced with a single-photon operator, it is known that single-photon BICs emerge due to destructive interference between multiple coupling points [34]. In our case, since two photons are created (or annihilated) at the same site, the resulting state has significant overlap with doublon modes. Thus, we expect a doublon BIC if the atomic level spacing Δ_1 lies within the doublon band.

To demonstrate this explicitly, we simulate a system of N=199 cavities, where a single GA couples to sites $x_{11}=99$ and $x_{12}=101$, i.e., a separation $\Delta x=2$. A doublon BIC arises due to destructive interference between emission paths [34], governed by the condition $1 + \exp(ik\Delta x) = 0$, which is satisfied with

$$k_{\rm DF} = \frac{(2n+1)\pi}{\Delta x}, \quad n \in \mathbb{N}.$$
 (8)

For $\Delta x=2$, this yields $k_{\rm DF}=\pm\pi/2$; the corresponding doublon frequency is $\omega_{\rm DF}=\omega_D(k_{\rm DF})$. Thus, setting $\Delta_1=\omega_{\rm DF}$ enables the formation of a doublon BIC, which is shown in Fig. 2(a) for U=10J and g=0.04J (chosen to remain in the Markovian regime).

We identify the BIC state $|\psi_b\rangle$ using the inverse participation ratio [78, 79]. Its overlap with the two-photon

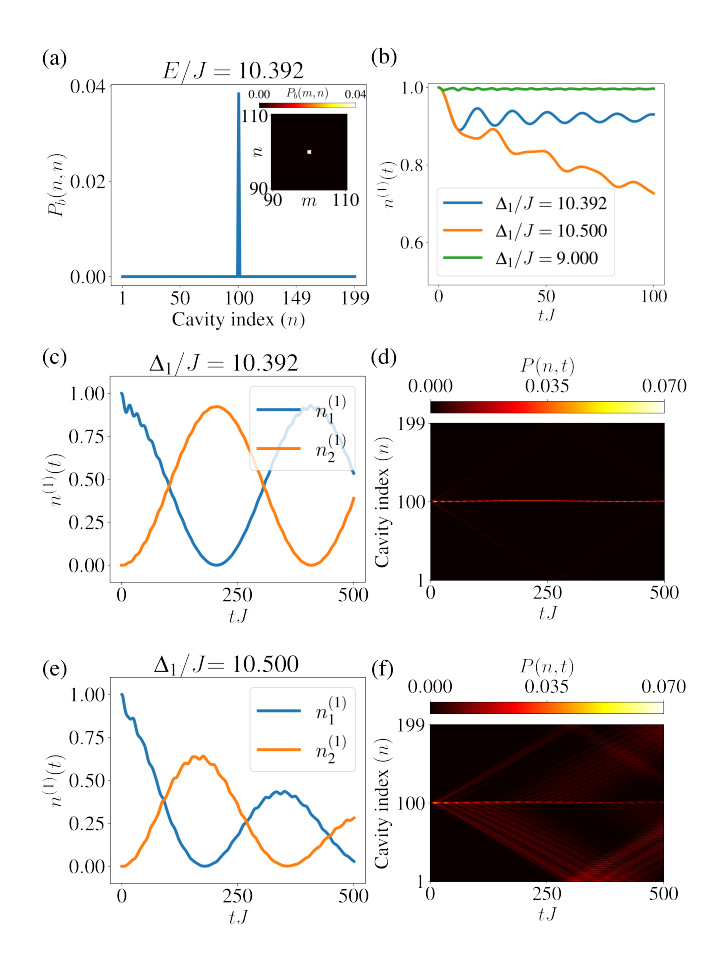


FIG. 2. Doublon BIC and DFI between GAs, for two-photon interaction [Eq. (7)]. Parameters: U=10J, g=0.04J, and $\Delta x=2$. (a) The doublon BIC for a single GA with the DF frequency $\Delta_1=10.392J.$ The plot shows the bound state's overlap $P_b(n,n)$ with the two-photon states $|0,nn\rangle$, while the inset also shows the off-diagonal elements $P_b(m,n)$. (b) Time evolution of the population $n^{(1)}(t)$ of the GA's $|1\rangle$ level for three values of Δ_1 : at the DF frequency (blue), inside the doublon band (orange), and outside the doublon band (green). (c) Population dynamics $n_{1,2}^{(1)}(t)$ of two braided GAs at the DF frequency. (d) Heatmap of the doublon population $P(n,t)=\langle \psi(t)|a_n^{\dagger}a_n^{\dagger}a_na_n|\psi(t)\rangle$ in the waveguide. (e, f) Same as in (c, d), but for a non-DF frequency inside the doublon band.

basis state $|0,mn\rangle = a_m^\dagger a_n^\dagger |\text{vac}\rangle$, denoted $P_b(m,n) = |\langle 0,mn|\psi_b\rangle|$, confirms that it is a doublon BIC: the overlap becomes exponentially small when $m \neq n$ [inset of Fig. 2(a)], a typical characteristic of a doublon; additionally, the wavefunction is localized in space, demonstrating its bound nature.

In Fig. 2(b), we plot the atom's $|1\rangle$ -level population $n^{(1)}(t) = \langle \psi(t) | \sigma^{(1),+} \sigma^{(1),-} | \psi(t) \rangle$ for three different atomic frequencies, starting from $|\psi(t=0)\rangle = \sigma^{(1),+}|\text{vac}\rangle$. When $\Delta_1 = \omega_{\text{DF}}$ (blue curve), this population stabilizes at a high value, typical of a BIC. In contrast, for Δ_1 within the doublon band (orange curve), the atom population displays exponential decay due to cou-

pling to radiative modes instead of the doublon BIC. For Δ_1 outside the doublon band (green curve), the atomic population shows decoherence-free behavior due to the formation of a bound state outside the continuum (BOC).

A key distinction between BICs and conventional BOCs is that BICs reside within the band, enabling significantly faster DFI between multiple GAs. To illustrate this, we add a second GA coupled to cavities 100 and 102, forming the braided configuration shown in Fig. 1(a). This configuration is known to be essential for enabling overlap between BICs associated with different atoms, a prerequisite for DFI [36, 51]. As shown in Fig. 2(c), starting from $|\psi(t=0)\rangle = \sigma_1^{(1),+}|\text{vac}\rangle$, this setup leads to coherent oscillations between the two atoms, except for a leakage at early times due to non-Markovian effects [49]. The corresponding doublon population in the waveguide $P(n,t) = \langle \psi(t) | a_n^{\dagger} a_n^{\dagger} a_n a_n | \psi(t) \rangle$ is visualized in Fig. 2(d), revealing no doublon leakage outside. In contrast, a slight detuning from $\omega_{\rm DF}$ not only suppresses the formation of BIC, but also allows partial population of the extended doublon modes. As a consequence, the DFI is disrupted [Fig. 2(e)] and doublon leakage into the waveguide becomes prominent [Fig. 2(f)].

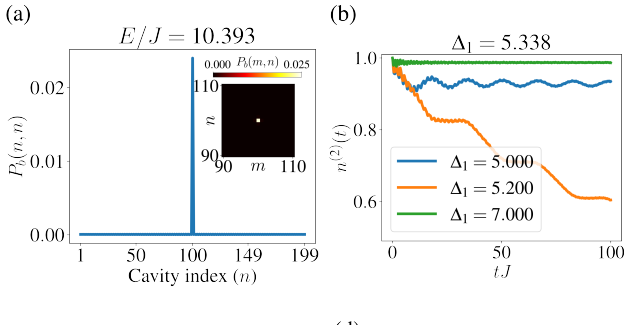
Single-photon coupling.—Above, we demonstrated the emergence of doublon BICs and the associated DFI between GAs coupled to a structured waveguide, using the direct two-photon coupling in Eq. (7). While that example is illustrative and conceptually clear, the two-photon coupling that it relies on generally requires external drives. We now turn to a more practical, and theoretically more intriguing, scenario based on common single-photon coupling with three-level GAs:

$$H_{\text{int}} = g \sum_{n=1}^{N_a} \sum_{i=1}^{p_n} \left[\sigma_n^{(1),+} a_{x_{nj}} + \sigma_n^{(2),+} a_{x_{nj}} + \text{H.c.} \right].$$
 (9)

Here, two-photon emission only becomes possible (through successive single-photon emission) when an atom is initialized in its $|2\rangle$ state, making the emergence of doublon BICs less intuitive and more conceptually rich.

To form a doublon BIC under the interaction in Eq. (9), the energy of the $|2\rangle$ level must match the doublon dispersion, i.e., $\Delta_1 + \Delta_2 \sim U$ [see Fig. 1(b)]. Additionally, to suppress single-photon emission into the waveguide, both transition energies must lie outside the single-photon band: $|\Delta_{1,2}| > 2J$. In this regime, the $|2\rangle$ state of the atom couples to doublon modes via a second-order process with an effective coupling strength $g_{\rm eff} \sim g^2/\Delta_2$ [79] to the doublon modes in the waveguide. This effective coupling is essential to the formation of doublon BICs in this setup. An additional effect of the second-order process is that it adds a Lamb shift to the energy of the $|2\rangle$ state and to the doublon dispersion [79].

At a decoherence-free frequency $\omega_{\rm DF} = \Delta_1 + \Delta_2 + \Delta$, this second-order process leads to the formation of a doublon BIC, as demonstrated in Fig. 3(a) for a single GA



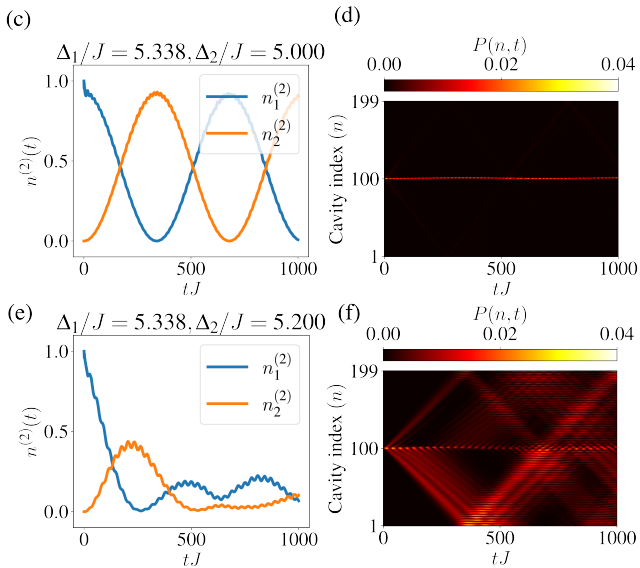


FIG. 3. Doublon BIC and DFI between GAs, for single-photon coupling [Eq. (9)]. Parameters: U=10J, g=0.25J, and $\Delta x=2$. (a) The doublon BIC for a single GA with the DF condition $\Delta_1=5.338J$ and $\Delta_2=5J$. The plot shows the diagonal overlap $P_b(n,n)$, indicating strong localization in real space. The inset shows the full two-photon amplitude $P_b(m,n)$, with vanishing off-diagonal elements confirming the doublon nature. (b) Time evolution of the population $n^{(2)}(t)$ of the GA's $|2\rangle$ level for fixed $\Delta_1=5.338J$ and varying Δ_2 : at the DF condition (blue), inside the doublon band (orange), and outside the doublon band (green). (c) Population dynamics $n_{1,2}^{(1)}(t)$ of two braided GAs at the DF frequency. (d) Heatmap of the doublon population $P(n,t)=\langle \psi(t)|a_n^{\dagger}a_n^{\dagger}a_na_n|\psi(t)\rangle$ in the waveguide. (e, f) Same as in (c, d), but for a non-DF frequency inside the doublon band.

with parameters g=0.25J, $\Delta_1=5.338J$, $\Delta_2=5J$, and $\Delta=0.054J$; the Δ is due to the Lamb shift in the atomic levels [79]. To confirm the BIC, we examine, in Fig. 3(b), the $|2\rangle$ -level occupation $n^{(2)}(t)=\langle \psi(t)|\sigma^{(2),+}\sigma^{(2),-}|\psi(t)\rangle/2$ for different atomic frequencies, , starting from $|\psi(t=0)\rangle=\sigma^{(2),+}\sigma^{(1),+}|\text{vac}\rangle/\sqrt{2}$. At $\Delta_1+\Delta_2+\Delta=\omega_{\text{DF}}$ (blue curve), we observe a decoherence-free behavior where the population stabilizes at a high value. The dynamics for $\Delta_1+\Delta_2+\Delta\neq\omega_{\text{DF}}$ inside (orange curve) and outside (green curve) the band are similar to those in Fig. 2(b), and distinct from

the BIC behavior.

We demonstrate the occurrence of DFI under this single-photon coupling in Fig. 3(c)-(d), where, as in Fig. 2(c)-(d), we add a second GA coupled to cavities 100 and 102, forming a braided configuration. Starting from $|\psi(t=0)\rangle = \sigma_1^{(2),+}\sigma_1^{(1),+}|\text{vac}\rangle/\sqrt{2}$, we observe coherent doublon-mediated dynamics between two GAs in the same way as in the preceding section. We see that due to the weaker effective coupling, the exchange rate between the GAs is slower than in Fig. 2(c) (even though q is larger in Fig. 3 than in Fig. 2). Consequently, the doublon population being exchanged in Fig. 3(d) is smaller than that in Fig. 2(d). Aside from these quantitative differences, the DFI behavior remains qualitatively the same as in the two-photon coupling case. A small detuning from the decoherence-free condition leads to the breakdown of DFI and leakage of doublons, as shown in Fig. 3(e)-(f), further confirming the role of doublon BICs in mediating the DFI.

Conclusion and outlook.—We have introduced giant atoms (GAs) coupled to non-linear structured waveguides as a platform to realize many-body bound states in the continuum (BICs), leveraging the destructive interference between spatially separated emission pathwaysan effect unique to GAs. We first demonstrated the formation of doublon BICs in setups with direct twophoton emission to the waveguide and showed that these BICs can mediate decoherence-free interactions (DFIs) between different GAs. We then extended our analysis to the more experimentally relevant case where only singlephoton emission is allowed and found that doublon BICs and their associated DFIs still emerge, enabled by virtual two-photon transitions. These findings highlight GAs as a versatile platform for realizing non-ergodic many-body states in open quantum systems and push forward interference as a powerful mechanism for engineering manybody BICs.

Experimentally, the required separation of doublon and free-photon dynamics (specifically, a nonlinear interaction strength $U \geq 4J$) is accessible in state-of-the-art platforms. In superconducting circuits, high-impedance resonators can yield $U/J \approx 24$ [80]. Additionally, giant atoms have been realized with transmon qubits coupled to arrays of superconducting resonators [71]. In coldatom systems, strong photon-photon interactions can be engineered via Rydberg blockade [81, 82], and recent proposals show that GA configurations can be realized in these platforms as well [37]. The observation and control of doublon BICs is thus experimentally feasible across a range of architectures.

The non-radiative nature of doublon BICs makes them promising candidates for entangled-state preparation [44] and fault-tolerant quantum gates in noisy environments [63, 83–85]. Their intrinsic many-body character enables applications beyond the single-excitation regime, such as preparing and distributing many-body

entangled states [86-89], and implementing unconventional quantum gates involving more than one photon [90, 91]. Looking ahead, the principles demonstrated here naturally extend to $N \geq 2$ many-body BICs [29] in GAs with more levels. These states could facilitate protected multi-qubit entanglement, robust many-body state transfer, and novel localization phenomena in open quantum systems. The interplay between photon-photon interactions and interference thus opens a rich frontier for both theoretical and experimental exploration of manybody BICs. Finally, our strategy is not limited to bosonic systems such as the Bose-Hubbard model, but can also be extended to interacting fermionic systems. Examples include two-magnon bound states in Ising-like XXZ chains [92–94], two-fermion bound states in the onedimensional Fermi-Hubbard model [95], and more complex many-body excitations such as Cooper pairs.

Acknowledgments.—All code used inwork this is open access via GitHub: https://github.com/WalterRieck/GiantAtoms. We thank Ariadna Soro and Xin Wang for fruitful discussions. G.C. is supported by the European Union's Horizon Europe programme HORIZON-MSCA-2023-PF-01-01 via the project 101146565 (SING-ATOM). A.F.K. acknowledges support from the Swedish Foundation for Strategic Research (grant numbers FFL21-0279 and FUS21-0063), the Horizon Europe programme HORIZON-CL4-2022-QUANTUM-01-SGA via the project 101113946 OpenSuperQPlus100, and from the Knut and Alice Wallenberg Foundation through the Wallenberg Centre for Quantum Technology (WACQT).

- * anton.frisk.kockum@chalmers.se † guangze@chalmers.se
- J. von Neumann and E. P. Wigner, Über merkwürdige diskrete eigenwerte, in *The Collected Works of Eugene Paul Wigner* (Springer Berlin Heidelberg, 1993) p. 291–293.
- [2] F. H. Stillinger and D. R. Herrick, Bound states in the continuum, Physical Review A 11, 446 (1975).
- [3] Y. Plotnik, O. Peleg, F. Dreisow, M. Heinrich, S. Nolte, A. Szameit, and M. Segev, Experimental Observation of Optical Bound States in the Continuum, Physical Review Letters 107, 183901 (2011).
- [4] M. Robnik, A simple separable Hamiltonian having bound states in the continuum, Journal of Physics A: Mathematical and General 19, 3845 (1986).
- [5] H. Friedrich and D. Wintgen, Interfering resonances and bound states in the continuum, Physical Review A 32, 3231 (1985).
- [6] D. C. Marinica, A. G. Borisov, and S. V. Shabanov, Bound States in the Continuum in Photonics, Physical Review Letters 100, 183902 (2008).
- [7] Y. Yang, C. Peng, Y. Liang, Z. Li, and S. Noda, Analytical Perspective for Bound States in the Continuum in Photonic Crystal Slabs, Physical Review Letters 113,

- 037401 (2014).
- [8] C. W. Hsu, B. Zhen, A. D. Stone, J. D. Joannopoulos, and M. Soljačić, Bound states in the continuum, Nature Reviews Materials 1, 16048 (2016).
- [9] K. Koshelev, A. Bogdanov, and Y. Kivshar, Engineering with Bound States in the Continuum, Optics and Photonics News 31, 38 (2020).
- [10] S. Joseph, S. Pandey, S. Sarkar, and J. Joseph, Bound states in the continuum in resonant nanostructures: an overview of engineered materials for tailored applications, Nanophotonics 10, 4175 (2021).
- [11] S. I. Azzam and A. V. Kildishev, Photonic Bound States in the Continuum: From Basics to Applications, Advanced Optical Materials 9, 2001469 (2021).
- [12] I. Deriy, I. Toftul, M. Petrov, and A. Bogdanov, Bound States in the Continuum in Compact Acoustic Resonators, Physical Review Letters 128, 084301 (2022).
- [13] H. Tong, S. Liu, M. Zhao, and K. Fang, Observation of phonon trapping in the continuum with topological charges, Nature Communications 11, 5216 (2020).
- [14] L. Carletti, K. Koshelev, C. De Angelis, and Y. Kivshar, Giant Nonlinear Response at the Nanoscale Driven by Bound States in the Continuum, Physical Review Letters 121, 033903 (2018).
- [15] Z. Liu, Y. Xu, Y. Lin, J. Xiang, T. Feng, Q. Cao, J. Li, S. Lan, and J. Liu, High-Q Quasibound States in the Continuum for Nonlinear Metasurfaces, Physical Review Letters 123, 253901 (2019).
- [16] K. Koshelev, Y. Tang, K. Li, D.-Y. Choi, G. Li, and Y. Kivshar, Nonlinear Metasurfaces Governed by Bound States in the Continuum, ACS Photonics 6, 1639 (2019).
- [17] L. Carletti, S. S. Kruk, A. A. Bogdanov, C. De Angelis, and Y. Kivshar, High-harmonic generation at the nanoscale boosted by bound states in the continuum, Physical Review Research 1, 023016 (2019).
- [18] A. P. Anthur, H. Zhang, R. Paniagua-Dominguez, D. A. Kalashnikov, S. T. Ha, T. W. W. Maß, A. I. Kuznetsov, and L. Krivitsky, Continuous Wave Second Harmonic Generation Enabled by Quasi-Bound-States in the Continuum on Gallium Phosphide Metasurfaces, Nano Letters 20, 8745 (2020).
- [19] G. Zograf, K. Koshelev, A. Zalogina, V. Korolev, R. Hollinger, D.-Y. Choi, M. Zuerch, C. Spielmann, B. Luther-Davies, D. Kartashov, S. V. Makarov, S. S. Kruk, and Y. Kivshar, High-Harmonic Generation from Resonant Dielectric Metasurfaces Empowered by Bound States in the Continuum, ACS Photonics 9, 567 (2022).
- [20] A. Kodigala, T. Lepetit, Q. Gu, B. Bahari, Y. Fainman, and B. Kanté, Lasing action from photonic bound states in continuum, Nature 541, 196 (2017).
- [21] S. T. Ha, Y. H. Fu, N. K. Emani, Z. Pan, R. M. Bakker, R. Paniagua-Domínguez, and A. I. Kuznetsov, Directional lasing in resonant semiconductor nanoantenna arrays, Nature Nanotechnology 13, 1042 (2018).
- [22] M. Wu, S. T. Ha, S. Shendre, E. G. Durmusoglu, W.-K. Koh, D. R. Abujetas, J. A. Sánchez-Gil, R. Paniagua-Domínguez, H. V. Demir, and A. I. Kuznetsov, Room-Temperature Lasing in Colloidal Nanoplatelets via Mie-Resonant Bound States in the Continuum, Nano Letters 20, 6005 (2020).
- [23] Y. Wang, Y. Fan, X. Zhang, H. Tang, Q. Song, J. Han, and S. Xiao, Highly Controllable Etchless Perovskite Microlasers Based on Bound States in the Continuum, ACS Nano 15, 7386 (2021).

- [24] F. Yesilkoy, E. R. Arvelo, Y. Jahani, M. Liu, A. Tittl, V. Cevher, Y. Kivshar, and H. Altug, Ultrasensitive hyperspectral imaging and biodetection enabled by dielectric metasurfaces, Nature Photonics 13, 390 (2019).
- [25] S. Romano, G. Zito, S. N. Lara Yépez, S. Cabrini, E. Penzo, G. Coppola, I. Rendina, and V. Mocellaark, Tuning the exponential sensitivity of a bound-statein-continuum optical sensor, Optics Express 27, 18776 (2019).
- [26] M. L. Tseng, Y. Jahani, A. Leitis, and H. Altug, Dielectric Metasurfaces Enabling Advanced Optical Biosensors, ACS Photonics 8, 47 (2020).
- [27] H. Altug, S.-H. Oh, S. A. Maier, and J. Homola, Advances and applications of nanophotonic biosensors, Nature Nanotechnology 17, 5 (2022).
- [28] Y. Chen, C. Zhao, Y. Zhang, and C.-w. Qiu, Integrated Molar Chiral Sensing Based on High-Q Metasurface, Nano Letters 20, 8696 (2020).
- [29] S. Sugimoto, Y. Ashida, and M. Ueda, Many-Body Bound States in the Continuum (2023), arXiv:2307.05456.
- [30] J. M. Zhang, D. Braak, and M. Kollar, Bound States in the Continuum Realized in the One-Dimensional Two-Particle Hubbard Model with an Impurity, Physical Review Letters 109, 116405 (2012).
- [31] Y. Ashida, T. Yokota, A. m. c. İmamoğlu, and E. Demler, Nonperturbative waveguide quantum electrodynamics, Physical Review Research 4, 023194 (2022).
- [32] N. Sun, W. Zhang, H. Yuan, and X. Zhang, Boundary-localized many-body bound states in the continuum, Communications Physics 7, 299 (2024).
- [33] A. F. Kockum, Quantum Optics with Giant Atoms the First Five Years, in *International Symposium on Mathe*matics, Quantum Theory, and Cryptography (Mathematics for Industry, vol 33) (Springer, 2021) pp. 125–146.
- [34] A. Frisk Kockum, P. Delsing, and G. Johansson, Designing frequency-dependent relaxation rates and Lamb shifts for a giant artificial atom, Physical Review A 90, 013837 (2014).
- [35] L. Guo, A. L. Grimsmo, A. F. Kockum, M. Pletyukhov, and G. Johansson, Giant acoustic atom: A single quantum system with a deterministic time delay, Physical Review A 95, 053821 (2017).
- [36] A. F. Kockum, G. Johansson, and F. Nori, Decoherence-Free Interaction between Giant Atoms in Waveguide Quantum Electrodynamics, Physical Review Letters 120, 140404 (2018).
- [37] A. González-Tudela, C. S. Muñoz, and J. I. Cirac, Engineering and Harnessing Giant Atoms in High-Dimensional Baths: A Proposal for Implementation with Cold Atoms, Physical Review Letters 122, 203603 (2019).
- [38] L. Guo, A. F. Kockum, F. Marquardt, and G. Johansson, Oscillating bound states for a giant atom, Physical Review Research 2, 043014 (2020).
- [39] P. O. Guimond, B. Vermersch, M. L. Juan, A. Sharafiev, G. Kirchmair, and P. Zoller, A unidirectional on-chip photonic interface for superconducting circuits, npj Quantum Information 6, 32 (2020).
- [40] A. Ask, Y.-L. L. Fang, and A. F. Kockum, Synthesizing electromagnetically induced transparency without a control field in waveguide QED using small and giant atoms (2020), arXiv:2011.15077.

- [41] D. Cilluffo, A. Carollo, S. Lorenzo, J. A. Gross, G. M. Palma, and F. Ciccarello, Collisional picture of quantum optics with giant emitters, Physical Review Research 2, 043070 (2020).
- [42] X. Wang, T. Liu, A. F. Kockum, H.-R. Li, and F. Nori, Tunable Chiral Bound States with Giant Atoms, Physical Review Letters 126, 043602 (2021).
- [43] L. Du and Y. Li, Single-photon frequency conversion via a giant Λ-type atom, Physical Review A 104, 023712 (2021).
- [44] A. Soro and A. F. Kockum, Chiral quantum optics with giant atoms, Physical Review A 105, 023712 (2022).
- [45] X. Wang and H.-r. Li, Chiral quantum network with giant atoms, Quantum Science and Technology 7, 035007 (2022).
- [46] L. Du, Y. Zhang, J. H. Wu, A. F. Kockum, and Y. Li, Giant Atoms in a Synthetic Frequency Dimension, Physical Review Letters 128, 223602 (2022).
- [47] L. Du, Y.-T. Chen, Y. Zhang, and Y. Li, Giant atoms with time-dependent couplings, Physical Review Research 4, 023198 (2022).
- [48] S. Terradas-Briansó, C. A. González-Gutiérrez, F. Nori, L. Martín-Moreno, and D. Zueco, Ultrastrong waveguide QED with giant atoms, Physical Review A 106, 063717 (2022).
- [49] A. Soro, C. S. Muñoz, and A. F. Kockum, Interaction between giant atoms in a one-dimensional structured environment, Physical Review A 107, 013710 (2023).
- [50] L. Du, L. Guo, Y. Zhang, and A. F. Kockum, Giant emitters in a structured bath with non-Hermitian skin effect, Physical Review Research 5, L042040 (2023).
- [51] E. R. Ingelsten, A. F. Kockum, and A. Soro, Avoiding decoherence with giant atoms in a two-dimensional structured environment (2024), arXiv:2402.10879.
- [52] L. Leonforte, X. Sun, D. Valenti, B. Spagnolo, F. Illuminati, A. Carollo, and F. Ciccarello, Quantum optics with giant atoms in a structured photonic bath, Quantum Science and Technology 10, 015057 (2025).
- [53] X. Wang, H.-B. Zhu, T. Liu, and F. Nori, Realizing quantum optics in structured environments with giant atoms, Physical Review Research 6, 013279 (2024).
- [54] F. Roccati and D. Cilluffo, Controlling Markovianity with Chiral Giant Atoms, Physical Review Letters 133, 063603 (2024).
- [55] R.-Y. Gong, Z.-Y. He, C.-H. Yu, G.-F. Zhang, F. Nori, and Z.-L. Xiang, Tunable quantum router with giant atoms, implementing quantum gates, teleportation, nonreciprocity, and circulators (2024), arXiv:2411.19307.
- [56] L. Du and A. F. Kockum, Unconventional and robust light-matter interactions based on the non-Hermitian skin effect, Physical Review Research 7, 013140 (2025).
- [57] L. Du, X. Wang, A. F. Kockum, and J. Splettstoesser, Dressed Interference in Giant Superatoms: Entanglement Generation and Transfer (2025), arXiv:2504.12942.
- [58] M. V. Gustafsson, T. Aref, A. F. Kockum, M. K. Ekström, G. Johansson, and P. Delsing, Propagating phonons coupled to an artificial atom, Science 346, 207 (2014).
- [59] R. Manenti, A. F. Kockum, A. Patterson, T. Behrle, J. Rahamim, G. Tancredi, F. Nori, and P. J. Leek, Circuit quantum acoustodynamics with surface acoustic waves, Nature Communications 8, 975 (2017).
- [60] K. J. Satzinger, Y. P. Zhong, H.-S. Chang, G. A. Peairs, A. Bienfait, M.-H. Chou, A. Y. Cleland, C. R. Conner,

- É. Dumur, J. Grebel, I. Gutierrez, B. H. November, R. G. Povey, S. J. Whiteley, D. D. Awschalom, D. I. Schuster, and A. N. Cleland, Quantum control of surface acoustic-wave phonons, Nature **563**, 661 (2018).
- [61] A. Bienfait, K. J. Satzinger, Y. P. Zhong, H.-S. Chang, M.-H. Chou, C. R. Conner, É. Dumur, J. Grebel, G. A. Peairs, R. G. Povey, and A. N. Cleland, Phonon-mediated quantum state transfer and remote qubit entanglement, Science 364, 368 (2019).
- [62] G. Andersson, B. Suri, L. Guo, T. Aref, and P. Delsing, Non-exponential decay of a giant artificial atom, Nature Physics 15, 1123 (2019).
- [63] B. Kannan, M. J. Ruckriegel, D. L. Campbell, A. Frisk Kockum, J. Braumüller, D. K. Kim, M. Kjaergaard, P. Krantz, A. Melville, B. M. Niedzielski, A. Vepsäläinen, R. Winik, J. L. Yoder, F. Nori, T. P. Orlando, S. Gustavsson, and W. D. Oliver, Waveguide quantum electrodynamics with superconducting artificial giant atoms, Nature 583, 775 (2020).
- [64] A. Bienfait, Y. P. Zhong, H.-S. Chang, M.-H. Chou, C. R. Conner, É. Dumur, J. Grebel, G. A. Peairs, R. G. Povey, K. J. Satzinger, and A. N. Cleland, Quantum Erasure Using Entangled Surface Acoustic Phonons, Physical Review X 10, 021055 (2020).
- [65] G. Andersson, M. K. Ekström, and P. Delsing, Electromagnetically Induced Acoustic Transparency with a Superconducting Circuit, Physical Review Letters 124, 240402 (2020).
- [66] A. M. Vadiraj, A. Ask, T. G. McConkey, I. Nsanzineza, C. W. S. Chang, A. F. Kockum, and C. M. Wilson, Engineering the level structure of a giant artificial atom in waveguide quantum electrodynamics, Physical Review A 103, 023710 (2021).
- [67] Z. Q. Wang, Y. P. Wang, J. Yao, R. C. Shen, W. J. Wu, J. Qian, J. Li, S. Y. Zhu, and J. Q. You, Giant spin ensembles in waveguide magnonics, Nature Communications 13, 7580 (2022).
- [68] C. Joshi, F. Yang, and M. Mirhosseini, Resonance Fluorescence of a Chiral Artificial Atom, Physical Review X 13, 021039 (2023).
- [69] J. Hu, D. Li, Y. Qie, Z. Yin, A. F. Kockum, F. Nori, and S. An, Engineering the Environment of a Superconducting Qubit with an Artificial Giant Atom (2024), arXiv:2410.15377.
- [70] A. Almanakly, B. Yankelevich, M. Hays, B. Kannan, R. Assouly, A. Greene, M. Gingras, B. M. Niedzielski, H. Stickler, M. E. Schwartz, K. Serniak, J. Î.-j. Wang, T. P. Orlando, S. Gustavsson, J. A. Grover, and W. D. Oliver, Deterministic remote entanglement using a chiral quantum interconnect, Nature Physics 21, 825 (2025).
- [71] V. Jouanny, L. Peyruchat, M. Scigliuzzo, A. Mercurio, E. Di Benedetto, D. De Bernardis, D. Sbroggiò, S. Frasca, V. Savona, F. Ciccarello, and P. Scarlino, Superstrong Dynamics and Chiral Emission of a Giant Atom in a Structured Bath (2025), arXiv:2509.01579.
- [72] S. Guo, Y. Wang, T. Purdy, and J. Taylor, Beyond spontaneous emission: Giant atom bounded in the continuum, Physical Review A 102, 033706 (2020).
- [73] K. Winkler, G. Thalhammer, F. Lang, R. Grimm, J. Hecker Denschlag, A. J. Daley, A. Kantian, H. P. Büchler, and P. Zoller, Repulsively bound atom pairs in an optical lattice, Nature 441, 853 (2006).
- [74] R. Piil and K. Mølmer, Tunneling couplings in discrete

- lattices, single-particle band structure, and eigenstates of interacting atom pairs, Physical Review A **76**, 023607 (2007).
- [75] Z. Wang, T. Jaako, P. Kirton, and P. Rabl, Supercorrelated Radiance in Nonlinear Photonic Waveguides, Physical Review Letters 124, 213601 (2020).
- [76] M. A. Gorlach and A. N. Poddubny, Topological edge states of bound photon pairs, Physical Review A 95, 053866 (2017).
- [77] M. Ayyash, X. Xu, S. Ashhab, and M. Mariantoni, Driven multiphoton qubit-resonator interactions, Physical Review A 110, 053711 (2024).
- [78] F. Wegner, Inverse participation ratio in 2+ε dimensions, Zeitschrift für Physik B Condensed Matter 36, 209 (1980).
- [79] See Supplemental Material at [url], which includes Refs. [78, 96], for additional information on the (i) numerical details and (ii) an analytical derivation of the effective model.
- [80] S. Andersson, H. Havir, A. Ranni, S. Haldar, and V. F. Maisi, High-impedance microwave resonators with twophoton nonlinear effects, Nature Communications 16, 552 (2025).
- [81] A. V. Gorshkov, J. Otterbach, M. Fleischhauer, T. Pohl, and M. D. Lukin, Photon-Photon Interactions via Rydberg Blockade, Physical Review Letters 107, 133602 (2011).
- [82] T. Peyronel, O. Firstenberg, Q.-Y. Liang, S. Hofferberth, A. V. Gorshkov, T. Pohl, M. D. Lukin, and V. Vuletić, Quantum nonlinear optics with single photons enabled by strongly interacting atoms, Nature 488, 57 (2012).
- [83] G. Chen and A. Frisk Kockum, Simulating open quantum systems with giant atoms, Quantum Science and Technology 10, 025028 (2025).
- [84] G. Chen and A. F. Kockum, Scalable quantum simulator with an extended gate set in giant atoms (2025), arXiv:2503.04537.
- [85] G. Chen and A. F. Kockum, Efficient three-qubit gates with giant atoms (2025), arXiv:2510.04545.
- [86] W. Dür, H. Aschauer, and H.-J. Briegel, Multiparticle Entanglement Purification for Graph States, Physical Review Letters 91, 107903 (2003).
- [87] H.-J. Briegel, W. Dür, J. I. Cirac, and P. Zoller, Quantum Repeaters: The Role of Imperfect Local Operations in Quantum Communication, Physical Review Letters 81, 5932 (1998).
- [88] S. Wehner, D. Elkouss, and R. Hanson, Quantum internet: A vision for the road ahead, Science 362, eaam9288 (2018).
- [89] N. Sangouard, C. Simon, H. de Riedmatten, and N. Gisin, Quantum repeaters based on atomic ensembles and linear optics, Reviews of Modern Physics 83, 33 (2011).
- [90] T. Caneva, M. T. Manzoni, T. Shi, J. S. Douglas, J. I. Cirac, and D. E. Chang, Quantum dynamics of propagating photons with strong interactions: a generalized input-output formalism, New Journal of Physics 17, 113001 (2015).
- [91] H. J. Kimble, The quantum internet, Nature 453, 1023 (2008).
- [92] N. Papanicolaou and G. C. Psaltakis, Bethe ansatz for two-magnon bound states in anisotropic magnetic chains of arbitrary spin, Physical Review B 35, 342 (1987).
- [93] N. Wu, H. Katsura, S.-W. Li, X. Cai, and X.-W. Guan, Exact solutions of few-magnon problems in the spin-S pe-

- riodic XXZ chain, Physical Review B ${f 105},$ 064419 (2022). [94] M. Takahashi, Thermodynamics of One-Dimensional
- Solvable Models (Cambridge University Press, 1999).
- [95] F. H. L. Essler, H. Frahm, F. Göhmann, A. Klümper,
- and V. E. Korepin, *The One-Dimensional Hubbard Model* (Cambridge University Press, 2005).
- [96] X. Wang, J.-Q. Li, Z. Wang, A. F. Kockum, L. Du, T. Liu, and F. Nori, Nonlinear chiral quantum optics with giant-emitter pairs (2024), arXiv:2404.09829.

Supplemental Material for "Doublon bound states in the continuum through giant atoms"

Walter Rieck, Anton Frisk Kockum, ** and Guangze Chen**, **

¹Department of Microtechnology and Nanoscience, Chalmers University of Technology, 41296 Gothenburg, Sweden

(Dated: November 25, 2025)

I. NUMERICAL DETAILS

In the main text, we defined the full Hamiltonian of the system (N_a giant atoms interacting with a waveguide consisting of N cavities at p_n coupling points for atom n) in Eqs. (1), (2), (4), and (9) (for the excitation-number-conserving interaction Hamiltonian H_{int}):

$$H = H_A + H_B + H_{\text{int}},$$
(S1)
$$H_A = \sum_{n=1}^{N_a} \left[(\Delta_2 + \Delta_1) \frac{\sigma_n^{(2), +} \sigma_n^{(2), -}}{2} + \Delta_1 \sigma_n^{(1), +} \sigma_n^{(1), -} \right],$$
(S2)

$$H_B = \sum_{n=1}^{N} \frac{U}{2} a_n^{\dagger} a_n^{\dagger} a_n a_n - \sum_{n=1}^{N-1} J(a_n^{\dagger} a_{n+1} + \text{H.c.}), \quad (S3)$$

$$H_{\text{int}} = g \sum_{n=1}^{N_a} \sum_{j=1}^{p_n} \left[\sigma_n^{(1),+} a_{x_{nj}} + \sigma_n^{(2),+} a_{x_{nj}} + \text{H.c.} \right]. \quad (S4)$$

To perform numerical simulations for time evolution of the system with $N_a = 2$ giant atoms under this Hamiltonian, we first identify a complete basis for the system in the two-excitation subspace by enumerating all physically distinct states associated with each number of atomic excitations in this subspace:

- 1. For two atomic excitations and no photons, there are three distinct states: $|02,00\rangle$, $|20,00\rangle$, and $|11,00\rangle$.
- 2. For one atomic excitation and one photon in the waveguide, there are 2N states: $|10, n0\rangle$ and $|01, n0\rangle$ for each mode index n.
- 3. For no atomic excitations and two photons in the waveguide, we have N(N+1)/2 states of the form $|00,nm\rangle$, where $|00,nm\rangle \equiv |00,mn\rangle$ enforces symmetry under exchange.

The basis states here are explicitly defined as

$$\begin{split} |20,00\rangle &= \frac{\sigma_1^{(2),+}\sigma_1^{(1),+}}{\sqrt{2}}|\mathrm{vac}\rangle, \ |02,00\rangle &= \frac{\sigma_2^{(2),+}\sigma_2^{(1),+}}{\sqrt{2}}|\mathrm{vac}\rangle, \\ |11,00\rangle &= \sigma_1^{(1),+}\sigma_2^{(1),+}|\mathrm{vac}\rangle, \ |10,n0\rangle &= \sigma_1^{(1),+}a_n^\dagger|\mathrm{vac}\rangle, \\ |01,n0\rangle &= \sigma_2^{(1),+}a_n^\dagger|\mathrm{vac}\rangle, \ |00,nm\rangle &= a_n^\dagger a_m^\dagger|\mathrm{vac}\rangle. \end{split} \tag{S5}$$

Matrix elements of the Hamiltonian are computed by evaluating inner products between basis states and the Hamiltonian operator. For example,

$$\langle 20,00|H|20,00\rangle = \langle 20,00|H_A|20,00\rangle = \Delta_2 + \Delta_1.$$
 (S6)

We use Algorithm 1 to construct the Hamiltonian matrix numerically. By diagonalizing the constructed Hamiltonian, we obtain its eigenvalues and vectors. We then use the inverse participation ratio (IPR) to identify highly localized states that potentially are bound states in the continuum. The IPR for a state $|\psi\rangle$ is defined as [1]

$$IPR(|\psi\rangle) = \sum_{n} |\psi_n|^4,$$
 (S7)

where ψ_n is the amplitude of the nth basis state of the Hamiltonian. A value of IPR ≈ 1 indicates a highly localized state, while IPR $\approx 1/\sqrt{N}$ suggests a delocalized state. The BICs can therefore be found by locating the eigenstates that have the highest IPR values. In systems where BICs exist, the eigenstate with either the largest or second largest IPR typically corresponds to the BIC.

II. ANALYTICAL DERIVATION

Here we derive the effective Hamiltonian $H_{\rm eff}$ for a single giant atom coupled at two points to the structured waveguide with the excitation-number-conserving interaction Hamiltonian $H_{\rm int}$ given in Eq. (9) in the main text, such that Eqs. (S2)–(S4) are simplified to

$$H_{A} = \left[(\Delta_{2} + \Delta_{1}) \sigma^{(2),+} \sigma^{(2),-} + \Delta_{1} \sigma^{(1),+} \sigma^{(1),-} \right]$$

$$H_{B} = \sum_{n=1}^{N} \frac{U}{2} a_{n}^{\dagger} a_{n}^{\dagger} a_{n} a_{n} - \sum_{n=1}^{N-1} J(a_{n}^{\dagger} a_{n+1} + \text{H.c.})$$

$$H_{\text{int}} = g \sum_{i=1}^{2} \left[\sigma^{(1),+} a_{x_{j}} + \sigma^{(2),+} a_{x_{j}} + \text{H.c.} \right].$$
(S8)

where $x_{1,2}$ are the coupling-point coordinates of the atom. In particular, we are interested in the regime where the energy of the $|2\rangle$ level of the atom lies within the doublon band: $\Delta_1 + \Delta_2 \approx \omega_D(k)$. We therefore derive the effective Hamiltonian in the subspace spanned by the states $|2\rangle$ and $|\psi_D(k)\rangle$.

Since $H_{\rm int}$ does not directly couple these states (i.e., $\langle \psi_D(k)|H_{\rm int}|2\rangle=0$), the lowest non-zero contribution arises from second-order perturbation theory:

$$\langle \psi_D(k)|H_{\text{eff}}|2\rangle = \sum_m \frac{\langle \psi_D(k)|H_{\text{int}}|m\rangle\langle m|H_{\text{int}}|2\rangle}{\Delta_1 + \Delta_2 - E_m}$$
 (S9)

where $|m\rangle$ are eigenstates of $H_A + H_B$. To yield a non-zero contribution, both matrix elements in the numerator must be non-zero. The only such intermediate states $|m\rangle$ are $|1, k'\rangle = \sigma^{(1), +} a_{k'}^{\dagger} |\text{vac}\rangle$ with $E(k') = \Delta_1 + 2J \cos k'$.

We first Fourier transform the interaction Hamiltonian

$$H_{\text{int}} = \frac{g}{\sqrt{N}} \sum_{j=1}^{2} \sum_{k} \left[\sigma^{(1),+} + \sigma^{(2),+} \right] \exp(ikx_j) a_k + \text{H.c.},$$
(S10)

which gives

$$\langle 1, k' | H_{\text{int}} | 2 \rangle = \frac{\sqrt{2}g}{\sqrt{N}} \sum_{j=1}^{2} \exp(ik'x_j) := G(k').$$
 (S11)

To evaluate $\langle \psi_D(k)|H_{\rm int}|1,k'\rangle$, we note that:

$$|\psi_D(k)\rangle = \frac{1}{\sqrt{2}} \sum_{m=1}^N \sum_{n=1}^N e^{ik\frac{(m+n)}{2}} e^{-\frac{|m-n|}{\varsigma(k)}} a_m^{\dagger} a_n^{\dagger} |\text{vac}\rangle, \tag{S12}$$

where the localization length $\varsigma(k)$ is given by [2]

$$\varsigma(k) = -\left[\ln\left(\frac{\sqrt{U^2 + 16J^2\cos(k/2)^2} - U}{4J\cos(k/2)}\right)\right]^{-1}.$$
 (S13)

For large U, such as U=10J considered in the main text, the localization length $\varsigma(k)$ is sufficiently small [e.g., $\varsigma(\pi/2)\approx 0.506$] that we can approximate $\exp\left[-\frac{|m-n|}{\varsigma(k)}\right]$ as δ_{mn} , yielding

$$|\psi_D(k)\rangle = \frac{1}{\sqrt{2}} \sum_{n=1}^{N} \exp(ikn) a_n^{\dagger} a_n^{\dagger} |\text{vac}\rangle$$
 (S14)

and

$$\langle \psi_D(k)|H_{\text{int}}|1,k'\rangle = G^*(k-k'). \tag{S15}$$

Therefore, the second-order matrix element becomes

$$\langle \psi_D(k)|H_{\text{eff}}|2\rangle$$

$$= \sum_{k'} \frac{1}{\Delta_2 - 2J \cos k'} G(k - k') G(k')$$

$$= \frac{2g^2}{N} \sum_{k'} \frac{e^{ikx_1} + e^{ikx_2}}{\Delta_2 - 2J \cos k'}$$

$$+ \frac{2g^2}{N} \sum_{k'} \frac{e^{ikx_1} e^{ik'(x_2 - x_1)} + e^{ikx_2} e^{ik'(x_1 - x_2)}}{\Delta_2 - 2J \cos k'}.$$
(S16)

Due to the oscillation in k', the second term is suppressed, and the first term in Eq. (S16) dominates. In particular, at the decoherence-free wavevector $k = \pi/(x_2 - x_1)$, the second term vanishes. This yields

$$\langle \psi_D(k)|H_{\text{eff}}|2\rangle = g_{\text{eff}} \sum_{j=1}^{2} \exp(ikx_j),$$
 (S17)

where

$$g_{\text{eff}} = \frac{2g^2}{N} \sum_{kl} \frac{1}{\Delta_2 - 2J \cos k'}.$$
 (S18)

For the parameters used in Fig. 3(a–d) of the main text $(N = 199, U = 10J, g = 0.25J, \Delta_2 = 5J, \text{ and } x_2 - x_1 = 2)$, this effective coupling takes a value of $g_{\text{eff}} \approx 0.027J$.

The expression Eq. (S17) mirrors the single-photon matrix element

$$\langle vac|a_k H_{int}|1\rangle = g \sum_{i=1}^{2} exp(ikx_j),$$
 (S19)

except with $g \to g_{\text{eff}}$. The factor $\sum_{j=1}^{2} \exp(ikx_j)$, characteristic of giant atoms, gives rise to interference effects and underpins both bound states in the continuum (BICs) and decoherence-free interactions (DFIs).

In addition to the effective coupling, the second-order correction also induces a Lamb shift $\Delta_{\rm Lamb}$ in the $|2\rangle$ level:

$$\langle 2|H_{\text{eff}}|2\rangle = \sum_{k'} \frac{G(k')G^*(k')}{\Delta_2 - 2J\cos k'}$$

$$= \frac{2g^2}{N} \sum_{k'} \frac{1}{\Delta_2 - 2J\cos k'} \left| \sum_{j=1}^2 \exp(ik'x_j) \right|^2$$

$$= \frac{2g^2}{N} \sum_{k'} \frac{2 + 2\cos[k'(x_2 - x_1)]}{\Delta_2 - 2J\cos k'}.$$
(S20)

For the parameters used in Fig. 3(a–d) of the main text, this Lamb shift takes a value of $\Delta_{\text{Lamb}} \approx 0.057J$.

Finally, the doublon modes also get perturbed by H_{int} :

$$\langle \psi_D(k_1)|H_{\text{eff}}|\psi_D(k_2)\rangle$$

$$= \sum_{k'} \frac{G^*(k_1 - k')G(k_2 - k')}{\Delta_2 - 2J\cos k'}$$

$$= \frac{2g^2}{N} \sum_{k'} \frac{e^{i(k_2 - k_1)x_1} + e^{i(k_2 - k_1)x_2}}{\Delta_2 - 2J\cos k'}$$

$$+ \frac{2g^2}{N} \sum_{k'} \frac{e^{i(k_2 - k_1)x_1}e^{i(k_2 - k')(x_2 - x_1)}}{\Delta_2 - 2J\cos k'}$$

$$+ \frac{2g^2}{N} \sum_{k'} \frac{e^{i(k_2 - k_1)x_2}e^{i(k_2 - k')(x_1 - x_2)}}{\Delta_2 - 2J\cos k'},$$
(S21)

^{*} anton.frisk.kockum@chalmers.se

[†] guangze@chalmers.se

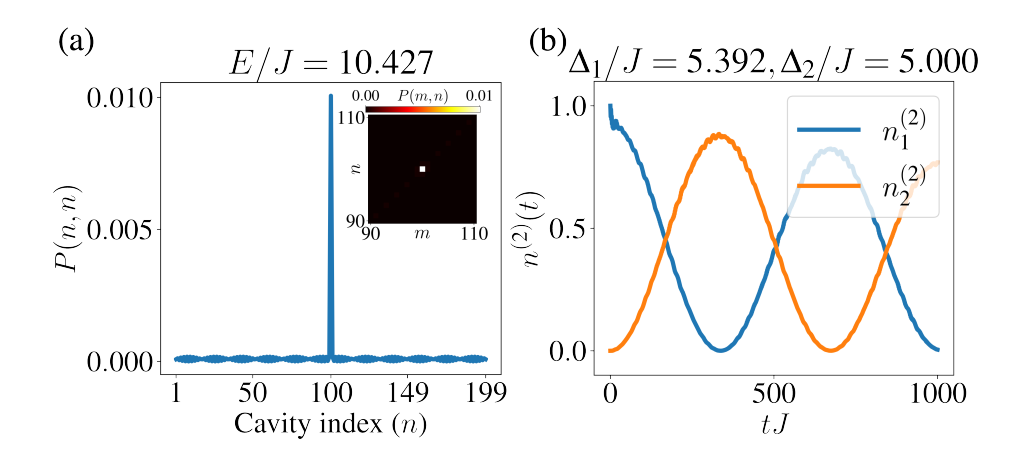


FIG. S1. Doublon BIC and DFI without accounting for the Lamb shift of the $|2\rangle$ level for U=10, g=0.25J, $\Delta x=2$, $\Delta_1=5.392$ and $\Delta_2=5$. (a) The doublon BIC for a single giant atom, where an extension of the bound state wavefunction outside the coupling points (99 and 101) can be seen, indicating that it is not a perfect bound state. (b) The corresponding DFI dynamics for two giant atoms, where the dynamics show a gradual decay of the total atomic population, due to the imperfect BIC.

which modifies both the doublon dispersion and the doublon eigenstates.

As a result, the decoherence-free condition also changes: satisfying $\Delta_1 + \Delta_2 = \omega_{\rm DF}$ is no longer sufficient. The corrected condition becomes

$$\Delta_1 + \Delta_2 + \Delta_{\text{Lamb}} = \omega_{\text{DF}} + \Delta_D(\omega_{\text{DF}})$$
 (S22)

where $\Delta_D(\omega_{\rm DF})$ is the perturbative shift in the doublon energy.

As shown in Fig. S1, choosing $\Delta_1 + \Delta_2 = \omega_{DF}$ fails

to produce a true BIC: the state energy is shifted, and the wavefunction spreads beyond the coupling region [Fig. S1(a)]. Correspondingly, the DFI quality deteriorates [Fig. S1(b)].

Numerically, we find that setting $\Delta_1 + \Delta_2 + \Delta = \omega_{\mathrm{DF}}$ with $\Delta = 0.054J$ results in the best decoherence-free quality for the parameters in Fig. 3 in the main text. The close match between Δ and Δ_{Lamb} indicates that H_{int} only has a minor effect on the doublon dispersion.

and F. Nori, Nonlinear chiral quantum optics with giant-emitter pairs (2024), arXiv:2404.09829.

^[1] F. Wegner, Inverse participation ratio in $2+\varepsilon$ dimensions, Zeitschrift für Physik B Condensed Matter **36**, 209 (1980).

^[2] X. Wang, J.-Q. Li, Z. Wang, A. F. Kockum, L. Du, T. Liu,

Algorithm 1: ConstructHamiltonian

```
1 Let D = \binom{N+N_a+1}{2};
  2 Initialize symmetric Hamiltonian H \in \mathbb{C}^{D \times D} with zeros, g[i][j] as the coupling strength of atom i at coupling point j,
       couplePoints[i] as the coupling point indices of atom i, and \Delta_1[i] and \Delta_2[i] as the level spacings associated with level 1
      and 2 respectively.
     // Set energy levels and couplings for |2\rangle
 3 for i = 0 to \binom{N_a+1}{2} - 1 do
          if i < N_a then
  4
               H[i,i] = \Delta_1[i] + \Delta_2[i];
  5
               for
each couplePoint, k in couplePoints[i] do
  6
                   j = {\binom{N_a+1}{2}} + iN + (\text{couplePoint} - 1);
  7
                   H[i,j] = \sqrt{2}g[i][k];
  8
          else
 9
               foreach 0 < j < k < N_a do
 10
                    if i == jN - j(j-1)/2 + k - j then L[i,i] = \Delta_1[j] + \Delta_1[k]
 11
 12
13 for i = 0 to N_a - 2 do
          for j = i + 1 to N_a - 1 do
14
               index = (i+1)N_a - i(i-1)/2 + j - 2i - 1;
15
               foreach (couplePoints, k) in couplePoints[i] do
16
                H[index, \binom{N_a+1}{2} + jN + couplePoint - 1] = g[i][k];
 17
               \begin{array}{l} \textbf{foreach} \text{ (couplePoint, k) in couplePoints[j]) } \textbf{do} \\ \bigsqcup H[\text{index}, \binom{N_a+1}{2} + jN + \text{couplePoint} - 1] = g[j][k]; \end{array}
18
 19
     // Set energy levels for couplings for |1\rangle
20 for i=0 to N_a-1 do
          for j = 0 to N - 1 do
21
               index = {\binom{N_a+1}{2}} + iN + j;
22
               H[index, index] = \Delta_1[i];
23
               if j \neq N-1 then
24
                H[index, index + 1] = -J;
 25
               iter = 0:
26
               foreach couplePoints in couplePoints[i] do
27
                    k = \text{couplePoint} - 1;
 28
                    if j \leq k then
 29
                     c_k = jN - j(j-1)/2 + k - j;
 30
 31
                     c_k = kN - k(k-1)/2 + j - k;
 32
                    H[\text{index}, c_k + {N_a \choose 2} + NN_a] = g[i][\text{iter}]
 33
                   if j == k then

\begin{bmatrix}
H[i, c_k + {N_a + 1 \choose 2} + NN_a] = g[i][\text{iter}]; \\
H[\text{index}, c_k + {N_a + 1 \choose 2} + NN_a] = \sqrt{2} \cdot g[i][\text{iter}];
\end{bmatrix}

 34
 35
 36
                   iter++
 37
     // Set energy levels and coupling for |0\rangle
38 for i = 0 to \binom{N+1}{2} - 1 do
39 | index = i + \binom{N_a+1}{2} + N_a N;
40
          for k = 0 to N - 1 do
               if i < kN - k(k-1)/2 then
c_k = i - N(k-1) + \frac{(k-2)(k-1)}{2} + (k-1), c_j = k-1;
41
 42
 43
                    break;
               else
44
                   c_k = N - 1, c_j = N - 1;
 45
          Determine neighbors of (c_j, c_k): (c_j \pm 1, c_k) and (c_j, c_k \pm 1);
46
          foreach valid neighbor (j', k') do
47
               c_{jk} = Nj' - j'(j'-1)/2 + k' - j';
48
               if j' = k' then
49
                   H[\text{index}, c_{jk}] = -\sqrt{2}J;

H[c_{jk}, c_{jk}] = U;
 50
 51
52
                   H[\text{index}, c_{jk}] = -J;
 53
```